Antiferromagnetic spin canting and magnetoelectric multipoles in h-YMnO₃

M. Ramakrishnan ®,[1,2,*] Y. Joly ®,[3] Q. N. Meier,[4] M. Fechner,[4] M. Porer,[1] S. Parchenko,[1] Y. W. Windsor,[1,†]
E. M. Bothschafter,[1] F. Lichtenberg,[4] and U. Staub[1,‡]

[1]*Swiss Light Source, Paul Scherrer Institut, 5232 Villigen PSI, Switzerland*
[2]*MAX IV Laboratory, Lund University, P.O. Box 118, SE-22100 Lund, Sweden*
[3]*Université Grenoble Alpes, Institut Néel, F-38042 Grenoble, France*
[4]*Department of Materials, ETH Zurich, 8093 Zurich, Switzerland*

Hexagonal YMnO₃ is a prototype antiferromagnet which exhibits multiferroic behavior with the ferroelectric and magnetic transitions occurring at different temperatures. We observe an out-of-plane canting of the Mn^{3+} magnetic moments using resonant x-ray diffraction (RXD) in a single crystal of this material. These canted moments result in the symmetry-forbidden (0,0,1) magnetic Bragg reflection, which is observed at the Mn $L_{2,3}$ absorption edges. We also observe an unexpected difference in the RXD spectral shapes at different temperatures. Using *ab initio* calculations, we explore the possibility that this behavior arises due to the interference between scattering from the canted magnetic moments and parity-odd atomic multipoles on the Mn^{3+} ions.

I. INTRODUCTION

Rapidly evolving technologies create a continuous demand for solid-state materials with one or more functionalities tailored for specific applications. An important category of single-phase multifunctional materials is that of magneto-electric multiferroics that possess spontaneous coexisting magnetic and ferroelectric orders [1–3]. Although a number of materials are known to have these properties, those with potential for real-world applications belong to a smaller subset which exhibit substantial coupling between their magnetic and electric properties. Moreover, the multiferroics which exhibit strong interactions between electric and magnetic orders have very complex microscopic coupling mechanisms [4], a deep understanding of which are essential to optimize their properties.

In-depth understanding of multiferroicity on a microscopic level requires a combination of exhaustive experiments and theoretical analyses, often employing computational tools such as density functional theory (DFT). Neutron scattering is the method of choice to understand magnetic structure and quantum mechanical interactions at the fundamental level, and techniques using photons from the terahertz to x-ray regimes offer a wealth of complementary information. X-ray spectroscopic techniques (like x-ray magnetic circular dichroism, for example) are being regularly used to determine element specific electronic and magnetic properties in multiferroics. Ideally, one needs a technique which combines spectroscopy with diffraction to examine the long-range order of certain fine aspects of electronic and magnetic structure in a comprehensive manner.

Resonant x-ray diffraction (RXD) is a technique that effectively combines diffraction with core-level absorption spectroscopy to observe long-range order in crystalline materials with element-specific electronic information. It has thus proved to be a useful tool to study fine details of magnetic arrangements and different types of magnetoelectric interactions in multiferroics over the years [4–7]. In standard RXD experiments, one obtains the long-range ordered electronic properties, such as magnetic dipoles and anisotropies in the electron density distribution (also referred to as orbital order), within the material system. However, combining RXD with *ab initio* calculations provides access to information regarding magnetic interactions, which are difficult to obtain using other experimental techniques [8–11]. In particular, RXD is sensitive to long-range-ordered localized multipoles, including the exotic magnetoelectric multipoles [12–14]. Magnetoelectric multipoles are ground-state localized entities which simultaneously break parity and time-reversal symmetries [9,12] and whose magnitudes and orientation in space can be calculated using DFT [15]. These multipoles have the appropriate symmetries to provide a single order-parameter in material systems lacking inversion and time-reversal [16]. More recently, it has also been suggested that they could be the order parameter for the pseudogap phase of high-temperature cuprate superconductors [14,17,18]. Even though a lot of

---
*mahesh.ramakrishnan@hotmail.com
†Present address: Institut für Optik und Atomare Physik, Technische Universität Berlin, Straße des 17. Juni 135, 10623 Berlin, Germany.
‡urs.staub@psi.ch

theoretical work has been performed on magnetoelectric multipoles [15,19–21], the lack of model systems where their presence can be indisputably confirmed using RXD experiments has hindered the progress in this field. In this study, we take advantage of the recent progress in the FDMNES code [22,23] which allows for a spherical tensor expansion of the scattering amplitudes contributing to a particular Bragg reflection as a function of energy, x-ray polarization, and azimuthal angle, to disentangle the various multipolar contributions in hexagonal $YMnO_3$ (h-YMO).

Hexagonal manganites with a general formula $RMnO_3$ (R = Y, In, Sc, Dy, Ho, Er, Tm, Yb, Lu) are one of the most studied classes of multiferroics. These are type-I multiferroics in which ferroelectricity sets in at a temperature T_C, which is well above the magnetic transition temperature T_N. Several types of antiferromagnetic orderings have been observed in compounds with different R atoms due to a complex interplay of geometrical frustration, spin-orbit coupling, lattice distortions and magnetic exchange interactions [3,24]. One prominent system of this family, h-YMO, crystallizes in the space group $P6_3/mmc$ at high temperatures and undergoes a geometrically driven ferroelectric transition around 1259 K, below which the symmetry changes to $P6_3cm$ [25]. The ferroelectricity in this material arises due to the buckling of the MnO_5 bipyramids [26,27], which is dissimilar to the displacement of the B-site cations seen in orthorhombic ABO_3 perovskites. The onset of magnetic order takes place at $T_N \approx 71K$, below which the Mn^{3+} moments order in a noncollinear arrangement with magnetic symmetry $P6_3'cm'$ [24,28,29].

Even though the ferroelectric and magnetic transitions in h-YMO occur independent of one another, anomalies are found in dielectric susceptibility at T_N indicating strong magnetoelectric coupling [30,31]. Magnetoelastic displacements of the Mn^{3+} ions have also been observed below T_N [32]. The d orbitals in the Mn^{3+} ions are strongly anisotropic, and hence, canting of the magnetic moments perpendicular to the *ab* plane are energetically favorable [33]. An indication of this spin-canting along the *c* axis has been obtained from optical measurements [34], but not in neutron scattering.

In this article, we present our resonant x-ray magnetic diffraction studies to observe possible spin cantings and magnetoelectric multipoles in h-YMO. The article is organized as follows. In Sec. II, the RXD experiment is described and basic results are analyzed. Detailed first-principles calculations of the RXD spectral profiles and magnetoelectric multipoles are described in Sec. IV, and the major outcomes are summarized in the concluding paragraphs.

II. EXPERIMENTAL DETAILS

A. Sample preparation and characterization

Crystalline hexagonal $YMnO_3$ was prepared by the optical floating zone melting technique using a Cyberstar mirror furnace [35]. Starting materials were powders of Y_2O_3 (Alfa Aesar, 99.99%, Lot B02X020) and Mn_2O_3 (MaTeck, 99.9%, Ch. 250708). Prior to the synthesis, the chemical composition of the Mn_2O_3 powder was confirmed by heating a small amount (about 70 mg) up to $1100\,°C$ at $10\,°C/min$ under a flow of synthetic air in a thermogravimetric analyzer (NET-

ZSCH TG 209 F1 Libra or NETZSCH STA449 C Jupiter) and observing the weight loss during the transformation of Mn_2O_3 into Mn_3O_4.

B. X-ray diffraction

The experiments were carried out at the endstation RE-SOXS [36] at the X11MA beamline [37] of the Swiss Light Source. The single crystal of size $4×4×2$ mm with the scattering surface along crystallographic *c* axis was mounted such that the [001] direction was along the horizontal scattering plane. Linear horizontal (π) and vertical (σ) polarized x-rays were focused at the sample with a spot-size of $130 × 50\,\mu m$. The beamline produced monochromatic x-rays with an energy resolution of about 0.15 eV and at the Mn $L_{2,3}$ edges. The sample was manually rotated in-situ with an accuracy of $±3°$ for the azimuthal angle (Ψ) scans. Reciprocal space scans along $(0, 0, L)$ were performed as a function of energy and temperature, with π polarized x-rays.

III. RESULTS AND INTERPRETATION

In h-YMO, the (0,0,1) Bragg reflection is forbidden according to the $P6_3cm$ space-group, but a strongly resonant diffraction signal was observed below the Néel temperature T_N. Figure 1 shows the reciprocal space scans along $(0, 0, L)$ showing an intense diffraction peak, where the maximum corresponds to a Bragg angle of about 55° at an energy of 642.75 eV. The apparent shift of the peak from $L = 1$ is likely due to refraction at the Mn L_3 resonance [38,39] The intensity of the reflection was found to reduce with increasing temperature and eventually go to zero at T_N, thereby proving its magnetic origin.

A. Origin of the forbidden Bragg reflection

To understand the nature of the magnetic form factor contributing to this Bragg reflection, the dependence of the scattering intensity on x-ray polarization and azimuthal angle was investigated. Figure 1 shows the ratio $I_\pi/(I_\sigma + I_\pi)$ of the (0,0,1) reflection as a function of the azimuthal angle Ψ. The intensity is independent of the azimuthal angle within experimental accuracy and has equal intensities in both polarization channels. The reflection also shows identical spectral shapes across the Mn $L_{2,3}$ edges with both σ- and π-polarized x rays. The precise nature of the magnetic moments (and/or other scattering tensors) contributing to this reflection can be understood by evaluating the structure factor. The structure factors, for a resonant Bragg reflection, can be written in the most general form as

$$S(h, k, l) = \sum_n f_n(E) e^{i2\pi(h\hat{x}+k\hat{y}+l\hat{z})\cdot\mathbf{r}_n}, \qquad (1)$$

where h, k, l are the Miller indices and n runs over all the resonant atoms (Mn) in the unit cell. In the magnetic unit cell (which is same as the structural unit cell in h-YMO), there are six Mn atoms—three atoms ($n = 1, 2, 3$) at $z = 0$ and three ($n = 4, 5, 6$) at $z = 0.5$, as shown in Fig. 1(c). For the (0,0,1) Bragg reflection with $h = k = 0$, Eq. (1) reduces to

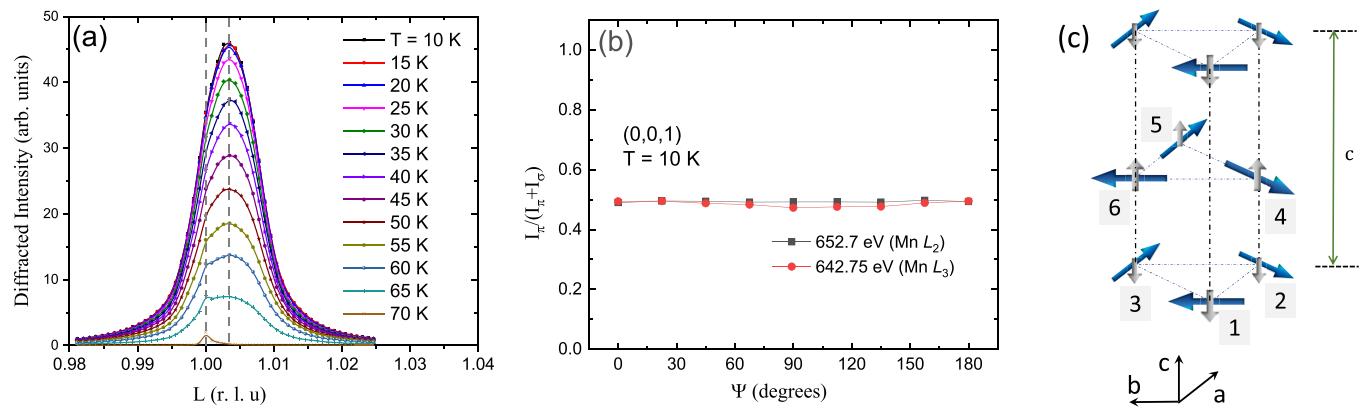$$S(0, 0, 1) = (f_1 + f_2 + f_3) - (f_4 + f_5 + f_6). \qquad (2)$$

FIG. 1. (a) Figure showing the magnetic (0,0,1) diffraction peak in h-YMO for various temperatures, measured at E = 642.75 eV (Mn L_3 edge) using π-polarized x-rays. The dashed vertical lines indicate the positions of the magnetic peak which undergoes refraction at the Mn L$_3$ edge and is consequently not centered exactly at $L = 1$, and the residual peak at 70 K which originates from the $\lambda/2$ leakage of the monochromator diffracting off the symmetry allowed (0,0,2) Bragg reflection. (b) Azimuthal dependence of the ratio $I_\pi/(I_\sigma + I_\pi)$ in h-YMO at $T = 10$ K, for the L_3 and L_2 edges of Mn. The error bars are within the symbols, and the solid lines are a guide to the eye. The inset shows the diffraction geometry. (c) The arrangement of in-plane magnetic moments (in blue) and the **c** axis canting (in gray). The length of the arrows do not represent the magnitude of the moments.

Since the scattering intensity is equal for both σ and π polarizations, the same structure factor is valid for both polarizations. As a first approximation, we look at the scattering terms within the form factor f_n, originating from the $E1E1$ process alone [40]. Here $E1$ refers to an electric dipole transition between the core and valence atomic levels involved (E stands for electric, and the number denotes the Δl between the atomic states. $E2$ and $M1$ would thus refer to an electric quadrupole and a magnetic dipole transition, respectively. Since RXD is a two-photon process, we always look at combinations of two transitions.) Equal intensities in both polarization channels ($I_\sigma = I_\pi$) and the absence of azimuthal dependence implies that

$$f_n \propto m_n^z \sin\theta, \qquad (3)$$

where m_n^z is the spin-component along the $\hat{\mathbf{z}}$ direction, also indicating scattering only in the rotated polarization channels ($\sigma \to \pi'$ and $\pi \to \sigma'$) [11,41]. Due to the negative sign in Eq. (2), only the antiferromagnetic (AFM) component of the spins contributes to the structure factor. In other words, the (0,0,1) reflection directly measures the AFM spin canting along the **c** axis of the crystal. An indication for such a spin-canting has been reported earlier from optical second-harmonic generation (SHG) studies [34]. Polarized neutrons are not sensitive to spin components along the Bragg wave vector. Hence, this AFM-canting of the Mn moments along the **c** axis does not contribute to any $(0, 0, L)$ type of reflections in neutron diffraction experiments. It should be noted that the magnetic (0,0,1) reflection which has been observed in neutron diffraction of h-HoMnO$_3$ [42] originates from the long-range ordering of the Ho^{3+} magnetic moments. This is unlike the case of Y^{3+} ions, which do not have ordered magnetic moments [28].

B. Spectral shape evolution with temperature

In the expression for the structure factor for the (0,0,1) magnetic Bragg reflection presented earlier, the energy dependence of the form factor was ignored. However, near an atomic absorption edge, the form factor $f_n(E)$ has a strong dependence on energy. The resulting energy dependence of the diffraction intensity at the absorption edge, called the spectral profile, contains detailed information regarding the symmetry and magnetoelectric interactions [11]. Hence, we measured the spectral profile of the magnetic (0,0,1) reflection for several temperatures (see Fig. 2). The spectra were obtained by integrating the intensity of the reciprocal space scans of the (0,0,1) reflection at every energy point around the Mn $L_{2,3}$ edges.

A striking observation is that the shape of the spectrum changes with temperature. For example, the relative intensity of the two peak-like features A and B at the Mn L_3 edge vary with temperature. This is also clearly seen in measurements of the scattered intensity for different energies with finer temperature steps. Figure 2(b) shows the intensity at each temperature normalized with respect to the intensity at the base temperature, for two different energies [corresponding to A and B Fig. 2(a)]. A detailed discussion about the origin of this observation is provided in the following section.

IV. DISCUSSION AND CALCULATIONS

A. Antiferromagnetic canting

The series of hexagonal manganites feature a wide variety of magnetic configurations whose origins have been extensively studied by a variety of techniques. Resonant x-ray diffraction at the Mn $L_{2,3}$ edges is sensitive to electronic ordering phenomena local to the Mn^{3+} ions. The (0,0,1) Bragg reflection, which is forbidden according to the $P6_3cm$ space group, shows strong resonant scattering below T_N. As seen in the previous section, this Bragg peak originates from the antiferromagnetic canting of spins along the **c** axis. This is yet another demonstration of the ability of RXD to investigate features like spin canting with high sensitivity. Notably, this type of spin canting is allowed under the previously inferred magnetic space group of this material ($P6_3'cm'$). It must be
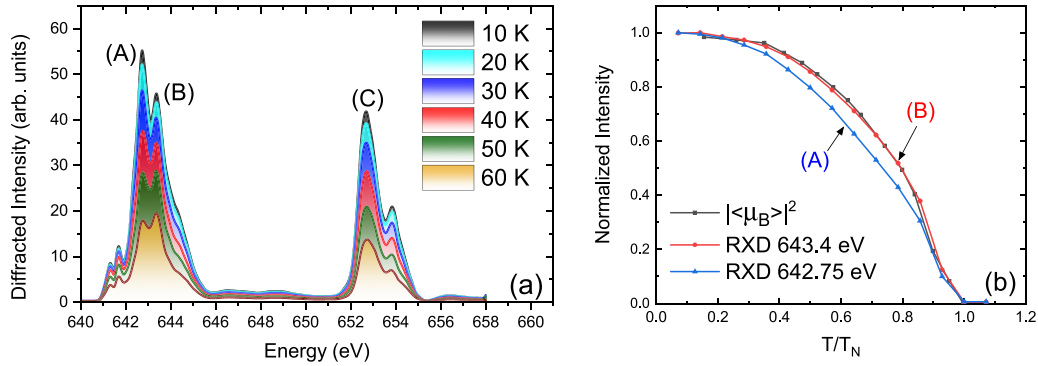
FIG. 2. (a) The spectral intensity profile of the (0,0,1) reflection at the Mn $L_{2,3}$ edges at various temperatures. (b) The temperature dependence of the diffraction intensity at the energies indicated A and B, and the square of the magnetic moment obtained in neutron diffraction (adapted with permission from Ref. [43] (copyrighted by the American Physical Society). The intensities have been normalized to unity at the lowest temperature. The solid lines are guides to the eye.

mentioned that since no other magnetic Bragg reflections are accessible at the Mn $L_{2,3}$ edges, it is not possible to obtain a quantitative estimate of the canting angle in this particular case. One possible way to measure this angle is by neutron diffraction where (H0L) type reflections are, in principle, sensitive to the canted part of the magnetic moment. Several Bragg reflections would be required to be collected with sufficient statistics to observe the expected small canting angle.

Even though there have even been indications of such a spin-canting from optical SHG experiments [34], it had not yet been reported in any scattering experiments. Spin-cantings in magnetoelectric systems are usually described by the antisymmetric exchange mechanism based on relativistic Dzyaloshinkii-Moriya (DM) interactions. The fact that we can observe a direct consequence of DM interactions using RXD makes it relevant from a fundamental perspective. Further details on the role of DM interactions in h-YMO can be found in Ref. [33] and the supplemental material of Ref. [44]. It would also be of fundamental interest to understand whether we can control the strength of the DM interactions and thereby, the canted moments using strain. Hence, one needs to repeat these experiments on differently strained epitaxial films, where the magnetic ordering temperature has been reported to change as a function of strain [45].

B. Changes in spectral shape

In Sec. III B, it was seen that the spectral shape of the (0,0,1) Bragg reflection was different for different temperatures. Changes in symmetry at the site of the resonant atom or its position in the unit cell can, in principle, alter the local electronic distribution affecting the RXD spectra [11]. However, it has been observed experimentally that movement of the Mn atoms within the unit cell occurs only at temperatures close to T_N, and, no structural changes have been observed below 40 K [32]. Hence, at temperatures below 40 K, any kind of atomic motion induced changes in spectral shape can be ruled out. Fine changes in the magnetic structure like the canting angle can also be ruled out since the temperature dependence of the (0,0,1) reflection coincides with the total magnetic moment in the system as observed with neutrons (see Fig. 2).

To understand other possible causes for this spectral change, we need to revisit the approximation made to arrive at Eq. (3), where we limited the form factor $f_n(E)$ to scattering terms originating from the $E1E1$ process. Higher-order electric ($E1E2$, $E2E2$) and mixed electric-magnetic processes ($E1M1$) have been found to contribute to resonant x-ray scattering in several correlated electron materials ($E2$: electric quadrupole transition, $M1$: magnetic dipole transition) [46]. Since scattering terms originating from different resonant processes can have different amplitudes and phases as a function of energy, the final spectral shape is the result of interference of all such contributions,

$$\begin{aligned} f_n(E) \propto\ & f_n^{E1E1}(E) + f_n^{E1E2}(E) \\ & + f_n^{E1M1}(E) + f_n^{E2E2}(E), \end{aligned} \tag{4}$$

where $f_n^{E1E1}(E) \propto m_n^z \sin\theta$ [given by Eq. (3)]. The higher-order terms $f_n^{E1E2}(E)$, $f_n^{E1M1}(E)$, and $f_n^{E2E2}(E)$ denote the combined form factor of all allowed multipoles from the respective processes. Only those multipoles which are long-range ordered with the Fourier component along the (0,0,1) wave vector contribute to this reflection [9,14,36]. Moreover, since there is no dependence of the scattering intensity on the azimuthal angle, the relevant atomic multipoles should also be symmetric with respect to any rotation about the *c* axis.

To investigate interference of one or more atomic multipoles in our experimental spectra, we look at the difference of the normalized spectra at 10 K and at 40 K. Figure 3 shows the the normalized spectra of the (0,0,1) reflection measured at 10K and 40K, and the difference spectral profile. The difference spectrum is obtained after normalizing the two spectra so that they have equal weight when integrating the intensity over the edges. The difference in these intensities can be attributed to the interference between terms of different origins in the scattering amplitude [10,47]. A quantitative evaluation is not feasible with the computational tools currently available. However, we employ a combination of DFT and phenomenology to provide a semi-quantitative description of this interference using a model of resonant scattering from the magnetoelectric multipoles.
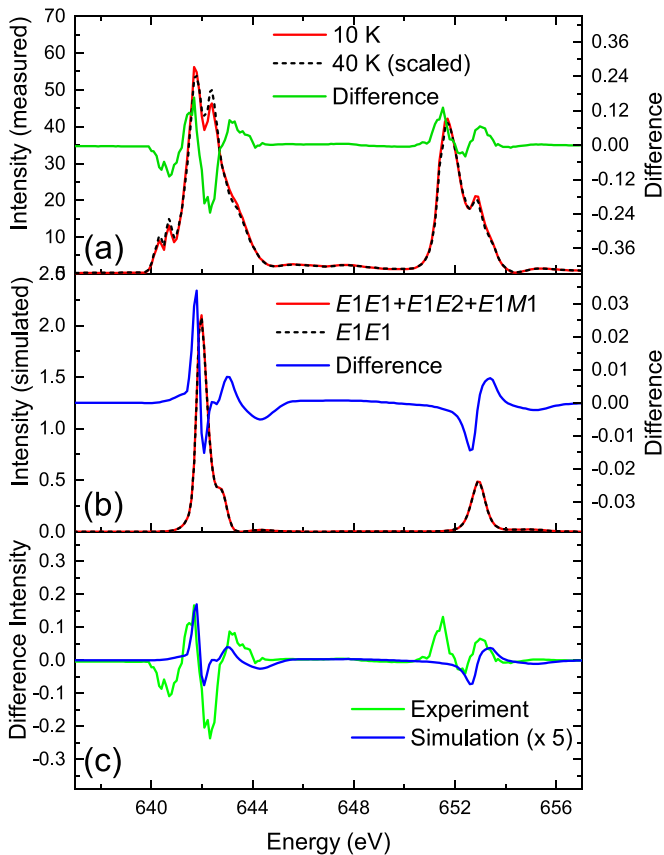
FIG. 3. (a) The normalized spectral shapes of the magnetic (0,0,1) reflection obtained at T = 10 K and T = 40 K. The intensities were normalized such that the difference spectrum averages to zero when integrated over the given energy range. (b) Spectral shapes obtained with and without contributions from magnetoelectric multipoles, calculated using FDMNES. In addition to $E1E1$, the $E1E2$ and $E1M1$ transition processes were also included in the calculation for the magnetoelectric multipoles. The difference between the two profiles is also shown in both panels. (c) The comparison of the experimental and calculated difference spectral profiles.

C. *Ab initio* calculations

The presence of higher-order multipoles in the scattering signal can be addressed using the *ab initio* FDMNES code [22,41]. The package uses a given crystal and starting magnetic structure to compute the spin-polarized density of states of a given material using density functional theory (DFT). Following this, the calculations for spectra for x-ray absorption and x-ray diffraction are performed. The code enables one to choose the transition processes for which the absorption or diffraction spectra are calculated. FDMNES does not compute the relaxed crystal structure, and hence, we used the crystal structure provided in Ref. [43]. The magnetic structure corresponding to the space group $P6_3'cm'$ given in Ref. [24] was used. To correlate with our findings, an antiferromagnetic canting of $1°$ was added to this input magnetic structure. The fully relativistic calculations were performed in the self-consistent mode using multiple scattering approach to obtain the magnetic ground state [22,23]. A cluster radius of 4 Å and a uniform broadening of 0.1 eV were used for all calculations.

The polarization resolved scattering intensities for the (0,0,1) Bragg reflection were calculated for $E1E1$ and a combination of $E1E1$, $E1E2$, and $E1M1$ processes, including correction factors for self absorption. Further details and a sample code are given in Ref. [48]. Due to inherent limitations in the estimation of core-hole effects and other interactions in the excited-state, the multiplet structure of the partially filled $3d$ orbitals are not accurately computed. Hence, the shapes of the spectra at the $L_{2,3}$ edges of Mn are not reproduced. However, we can get a semi-quantitative estimate of the relative scattering contributions from the magnetic canting and other higher-order multipoles.

For simplicity, we limit our calculations to the $E1E1$, $E1E2$, and $E1M1$ processes. Even though the latter processes are much weaker than $E1E1$, they can interfere amongst themselves giving visible changes in the spectral profiles. Including this interference, the total scattering intensity for a combination of the above processes can be approximated as

$$
\begin{aligned}
I^{\text{tot}}(E) &\propto \left| f_n^{E1E1}(E) + f_n^{E1E2}(E) \right. \\
&\quad \left. + f_n^{E1M1}(E) + f_n^{E2E2}(E) \right|^2, \\
&\approx \left| f_n^{E1E1}(E) \right|^2 + \left| f_n^{E1E1}(E) f_n^{E1E2}(E) \right| \\
&\quad + \left| f_n^{E1E1}(E) f_n^{E1M1}(E) \right|.
\end{aligned}
\tag{5}
$$

The squares and combinations of higher-order scattering terms can be neglected since they are generally too weak to be detected in such an experiment. The interference terms $\left| f_n^{E1E1}(E) . f_n^{E1E2}(E) \right|$ and $\left| f_n^{E1E1}(E) . f_n^{E1M1}(E) \right|$ enable us to observe the weak scattering from the higher-order multipoles. In the calculation using FDMNES, we can selectively calculate the scattering intensities from each process or any combinations of these (to account for any interference) [41]. Thus, we calculate the scattering intensities in case of (i) a $E1E1$ transition process alone, and (ii) combination of $E1E1$, $E1E2$, and $E1M1$ transition processes. We focus only on the scattered intensity in the rotated light channels for the (0,0,1) reflection, in accordance with experimental observations. The intensity in these channels for case (i) is exclusively the scattering due to the AFM canting of the magnetic dipole moments along the hexagonal **c** axis. For case (ii), the diffraction amplitudes from the higher-order multipoles interfere with the strong scattering signal from the canted AFM dipoles. On subtracting the spectra obtained for cases (i) and (ii) above, we observe a clear difference, of the order of a few percentage of the total diffraction intensity. As we can see, the calculations do not reproduce all features of the experimental spectra given in Fig. 3. The spectrum is shifted on the energy axis due to the inaccurate determination of the Fermi energy of the system in the presence of a core-hole. This difference spectrum along with the intensity profiles for calculations (i) and (ii) described above are plotted in Fig. 3. The difference spectrum obtained experimentally can now be compared with the calculated one [see Fig. 3(c)]. The mismatch between experiment and calculation is likely due to the fact that the effects like localization of electronic states in presence of the core-hole is not well accounted for in DFT-based calculations of $3d$ systems.

D. Multipolar analysis

In Sec. IV C, we established that the anomalous evolution of the spectral shapes with temperature can be explained by considering interference of scattering signals from the canted AFM dipoles and higher-order multipoles. The FDMNES code also allows the expansion of the scattering tensor in cartesian and/or spherical tensors, and to obtain the contribution of individual atomic multipoles. We expand the intensities as spherical tensors, and use the notation introduced in Refs. [9,49]. The atomic tensors derived from spherical harmonics are denoted by $\langle X_Q^K \rangle$, where X is the tensor type (T: parity-even and nonmagnetic; U: parity-odd and nonmagnetic, called polar multipoles; G: parity-odd and magnetic, called magnetoelectric multipoles), K is the rank of the tensor (0: monopolar, 1: dipolar, 2: quadrupolar, etc.) and Q is the projection of the tensor on the chosen basis. The multipolar contributions to the scattering intensity are shown in Fig. 4. The figure shows the absolute value of the form factor for all the nonzero multipoles obtained from $E1E1$, $E1E2$, and $E1M1$ processes as a function of energy, in the FDMNES calculation for h-YMO. The strongest scattering term is the *magnetoelectric octupole*, which is represented as $\langle G_3^3 \rangle - \langle G_{-3}^3 \rangle$. This spherical octupole resembles an f orbital which is symmetric with respect to rotations about the principal axis. In our calculations, the magnitude of the form factor corresponding to this octupole is about 1% of scattering from the magnetic dipole. One should note that even though the scattering intensities from the individual multipoles shown in the figure are small, they interfere with each other affecting the overall spectral shape significantly. Certain multipoles contribute to scattering in both the $E1E2$ and the $E1M1$ processes, albeit with different spectral shapes. For the Mn $L_{2,3}$ edges in h-YMO, the intensities resulting from the $E1E2$ process are generally stronger at these energies compared to those from $E1M1$, exemplified by the intensity of the magnetoelectric quadrupole $\langle G_0^2 \rangle$. However, to our knowledge, no experimental evaluation of the overall cross-sections of these two processes in RXD has been done to date. Yet another quantity of tremendous interest is $\langle G_0^0 \rangle$, which is a magnetic rank zero tensor. This entity, referred to as the magnetoelectric monopole or the magnetic charge, is fundamentally different from the monopole forbidden by classical electromagnetism [15]. It has nonzero intensity in our calculations, even though its contribution is weaker compared to the other multipoles.

One key aspect that has not been discussed so far concerns how interference of magnetoelectric terms leads to a different spectral shape at 40 K compared to 10 K. Ideally, one should calculate the RXD spectra as a function of temperature. There is a dearth of computational tools to quantitatively simulate the spectra for temperatures other than absolute zero. DFT-based methods are usually employed to deal with the ground state of a system. Due to the above reasons, we can only provide a phenomenological explanation for the observed temperature dependence of the RXD spectra. The temperature dependence of a purely magnetic term contributing to scattering can be measured in an experiment. Since the intensity of the (0,0,1) Bragg reflection in h-YMO is heavily dominated by magnetic scattering, we can assume its temperature
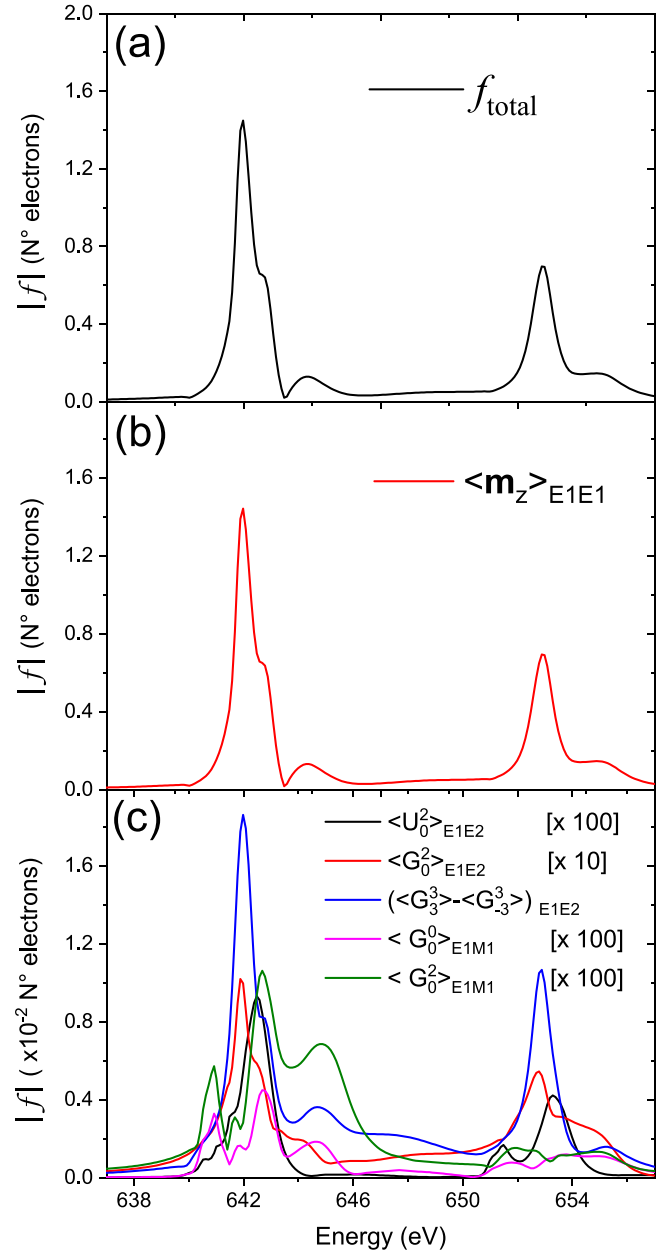

FIG. 4. Calculated spectral intensities for (a) the overall form factor of the (0,0,1) reflection in h-YMO obtained following interference of magnetic dipole and magnetoelectric multipoles, (b) the magnetic dipole term, and (c) the magnetoelectric $\langle G_Q^K \rangle$ multipoles at the Mn $L_{2,3}$ edges.

dependence to follow that of a pure magnetic dipole. Upon fitting the normalized intensity with a mean-field model $I \propto (T_N - T)^{2\beta_{\mathrm{mag}}}$, we obtain $\beta_{\mathrm{mag}} \approx 0.38$, where β_{mag} is the critical exponent of the magnetic scattering from the canted AFM moments. Magnetoelectric multipoles, on the other hand, are products of spatial and spin-density terms [15,46]. Therefore, they have distinct temperature dependencies, based on their actual tensorial form. Since the polar toroidal octupole is by far the strongest higher-order scattering term, we ignore the other multipoles to simplify our analysis. This octupole, which is a product of the spin density term and a spatial term
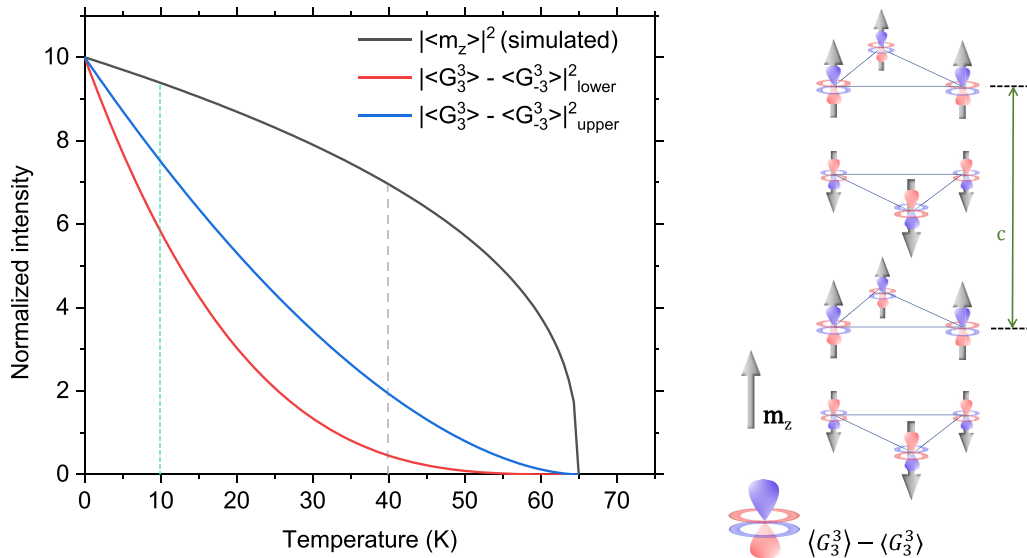
FIG. 5. Simulated temperature dependence of the intensity from magnetic scattering, and the predicted upper and lower bounds of scattering intensity from the magnetoelectric octupole $\langle G_3^3 \rangle - \langle G_{-3}^3 \rangle$ according to our phenomenological model. The dashed vertical lines at 10 K and 40 K are guides to the eye. The arrangement of the magnetoelectric octupoles and the c axis canted part of the magnetic moment are also shown (the in-plane moments are not shown).

to the power of two [46] can be approximated as

$$\left| \langle G_3^3 \rangle - \langle G_{-3}^3 \rangle \right| (T) \propto \mu(T)\, r^2(T), \tag{6}$$

where $\mu(T)$ and $r(T)$ are the temperature-dependent spin density and spatial terms. From literature, for spatially dependent electric polarization (like in ferroelectric materials) which depends linearly on $r(T)$, the value of the critical exponent β_r (critical exponent for the spatial dependence) falls within the range of 0.24 to 0.62 [50–52]. From Eq. (6), $\beta_{\mathrm{oct}} = \beta_{\mathrm{mag}} + 2\beta_r$ and hence, we can approximate the value of the overall critical exponent β_{oct} for the octupoles to be between 0.86 and 1.62. Based on these critical exponents, we can model the scattering intensity as a function of temperature for the magnetic dipole moments and octupoles as shown in Fig. 5. It is clear that the scattering contribution from magnetoelectric octupoles decreases at a comparatively higher rate with increasing temperature. Hence, the overall spectral shape is expected to change as a function of temperature and, for $T \approx 40$ K, one can assume that there is a relatively smaller contribution from $f_n^{E1E2}(E)$ and $f_n^{E1M1}(E)$ compared to $f_n^{E1E1}(E)$.

In RXD, the dipole-quadrupole $E1E2$ process is usually invoked in studies involving the pre-edge region of K edges of transition metals (where the $E2$ excitation $1s \rightarrow nd$ probes the partially filled d-states), or the L edges of rare-earths (where the $E2$ excitation $2p \rightarrow nf$ probes the f-states). The fact that we find a measurable cross-section for the $E1E2$ process at the Mn $L_{2,3}$ edges is very interesting from a fundamental perspective. For example, this could be due to a strong d-f hybridization leading to an f-like character of the final states. Note that this effect is visible due to the small spin canting leading to an effective c axis projection of the dipole moment that is approximately two orders of magnitude reduced in strength.

Earlier reports of changes in spectral shapes in resonant diffraction have occurred in systems with either atomic

motion or macroscopic changes like spin rotation [53]. In the absence of any of these observable changes, an observable change in the spectral shapes due to magnetoelectric multipoles is the most probable explanation. More investigations are needed to understand this phenomenon, complemented by dedicated theoretical and computational studies, ultimately to the comprehensive understanding of diffraction anomalous fine structure (DAFS) over large energy ranges in correlated electron materials.

V. SUMMARY

We investigate the (0,0,1) Bragg reflection below T_N in a single crystal of hexagonal YMnO₃ using resonant x-ray diffraction (RXD). Following a detailed examination of the dependence of diffraction intensity on x-ray polarization and azimuthal angle, we can conclude that this reflection, which is forbidden according to the $P6_3cm$ space-group, originates from an antiferromagnetic canting of the Mn^{3+} magnetic moments perpendicular to the crystallographic ab plane. We also observe that the shape of RXD spectra changes for different temperatures. Using *ab initio* calculations and phenomenological arguments, we discuss this behavior from the perspective of the interference between scattering from the magnetic dipole and parity-odd atomic multipoles on Mn ions. A detailed microscopic theory on the behavior of magnetoelectric multipoles at temperatures above absolute zero is necessary to validate our hypothesis and, in general, to expand the scope of this method in the broader field of multiferroics.

[1] N. A. Spaldin and M. Fiebig, The renaissance of magnetoelectric multiferroics, Science **309**, 391 (2005).

[2] D. I. Khomskii, Multiferroics: Different ways to combine magnetism and ferroelectricity, J. Magn. Magn. Mater. **306**, 1 (2006).

[3] M. Fiebig, T. Lottermoser, D. Meier, and M. Trassin, The evolution of multiferroics, Nat. Rev. Mater. **1**, 16046 (2016).

[4] M. Ramakrishnan, E. Constable, A. Cano, M. Mostovoy, J. S. White, N. Gurung, E. Schierle, S. de Brion, C. V. Colin, F. Gay, P. Lejay, E. Ressouche, E. Weschke, V. Scagnoli, R. Ballou, V. Simonet, and U. Staub, Field-induced double spin spiral in a frustrated chiral magnet, npj Quantum Mater. **4**, 60 (2019).

[5] S. B. Wilkins, T. R. Forrest, T. A. W. Beale, S. R. Bland, H. C. Walker, D. Mannix, F. Yakhou, D. Prabhakaran, A. T. Boothroyd, J. P. Hill, P. D. Hatton, and D. F. McMorrow, Nature of the Magnetic Order and Origin of Induced Ferroelectricity in TbMnO$_3$, Phys. Rev. Lett. **103**, 207602 (2009).

[6] H. C. Walker, F. Fabrizi, L. Paolasini, F. de Bergevin, J. Herrero-Martin, A. T. Boothroyd, D. Prabhakaran, and D. F. McMorrow, Femtoscale magnetically induced lattice distortions in multiferroic TbMnO$_3$, Science **333**, 1273 (2011).

[7] Y. W. Windsor, M. Ramakrishnan, L. Rettig, A. Alberca, E. M. Bothschafter, U. Staub, K. Shimamoto, Y. Hu, T. Lippert, and C. W. Schneider, Interplay between magnetic order at Mn and Tm sites alongside the structural distortion in multiferroic films of o-TmMnO$_3$, Phys. Rev. B **91**, 235144 (2015).

[8] D. Mannix, D. F. McMorrow, R. A. Ewings, A. T. Boothroyd, D. Prabhakaran, Y. Joly, B. Janousova, C. Mazzoli, L. Paolasini, and S. B. Wilkins, X-ray scattering study of the order parameters in multiferroic TbMnO$_3$, Phys. Rev. B **76**, 184420 (2007).

[9] S. W. Lovesey and V. Scagnoli, Chirality, magnetic charge and other strange entities in resonant x-ray bragg diffraction, J. Phys.: Condens. Matter **21**, 474214 (2009).

[10] V. E. Dmitrienko, E. N. Ovchinnikova, S. P. Collins, G. Nisbet, G. Beutier, Y. O. Kvashnin, V. V. Mazurenko, A. I. Lichtenstein, and M. I. Katsnelson, Measuring the Dzyaloshinskii-Moriya interaction in a weak ferromagnet, Nat. Phys. **10**, 202 (2014).

[11] M. Ramakrishnan, Y. Joly, Y. W. Windsor, L. Rettig, A. Alberca, E. M. Bothschafter, P. Lejay, R. Ballou, V. Simonet, V. Scagnoli, and U. Staub, Crystal symmetry lowering in chiral multiferroic Ba$_3$TaFe$_3$Si$_2$O$_{14}$ observed by x-ray magnetic scattering, Phys. Rev. B **95**, 205145 (2017).

[12] T. Arima, J.-H. Jung, M. Matsubara, M. Kubota, J.-P. He, Y. Kaneko, and Y. Tokura, Resonant magnetoelectric x-ray scattering in GaFeO$_3$: Observation of ordering of toroidal moments, J. Phys. Soc. Jpn. **74**, 1419 (2005).

[13] U. Staub, Y. Bodenthin, C. Piamonteze, M. Garcia-Fernandez, V. Scagnoli, M. Garganourakis, S. Koohpayeh, D. Fort, and S. W. Lovesey, Parity-and time-odd atomic multipoles in magnetoelectric GaFeO$_3$ as seen via soft x-ray Bragg diffraction, Phys. Rev. B **80**, 140410 (2009).

[14] V. Scagnoli, U. Staub, Y. Bodenthin, R. A. de Souza, M. Garcia-Fernandez, M. Garganourakis, A. T. Boothroyd, D. Prabhakaran, and S. W. Lovesey, Observation of orbital currents in CuO, Science **332**, 696 (2011).

[15] N. A. Spaldin, M. Fechner, E. Bousquet, A. Balatsky, and L. Nordström, Monopole-based formalism for the diagonal magnetoelectric response, Phys. Rev. B **88**, 094429 (2013).

[16] A. S. Zimmermann, D. Meier, and M. Fiebig, Ferroic nature of magnetic toroidal order, Nat. Commun. **5**, 4796 (2014).

[17] A. Shekhter and C. M. Varma, Considerations on the symmetry of loop order in cuprates, Phys. Rev. B **80**, 214501 (2009).

[18] M. Fechner, M. J. A. Fierz, F. Thöle, U. Staub, and N. A. Spaldin, Quasistatic magnetoelectric multipoles as order parameter for pseudogap phase in cuprate superconductors, Phys. Rev. B **93**, 174419 (2016).

[19] M. Fechner, N. A. Spaldin, and I. E. Dzyaloshinskii, Magnetic field generated by a charge in a uniaxial magnetoelectric material, Phys. Rev. B **89**, 184415 (2014).

[20] F. Thöle, M. Fechner, and N. A. Spaldin, First-principles calculation of the bulk magnetoelectric monopole density: Berry phase and Wannier function approaches, Phys. Rev. B **93**, 195167 (2016).

[21] Q. N. Meier, M. Fechner, T. Nozaki, M. Sahashi, Z. Salman, T. Prokscha, A. Suter, P. Schoenherr, M. Lilienblum, P. Borisov, I. E. Dzyaloshinskii, M. Fiebig, H. Luetkens, and N. A. Spaldin, Search for the Magnetic Monopole at a Magnetoelectric Surface, Phys. Rev. X **9**, 011011 (2019).

[22] Y. Joly, X-ray absorption near-edge structure calculations beyond the muffin-tin approximation, Phys. Rev. B **63**, 125120 (2001).

[23] Y. Joly, S. D. Matteo, and O. Bunau, Resonant x-ray diffraction: Basic theoretical principles, Eur. Phys. J.: Spec. Top. **208**, 21 (2012).

[24] P. J. Brown and T. Chatterji, Neutron diffraction and polarimetric study of the magnetic and crystal structures of HoMnO$_3$ and YMnO$_3$, J. Phys.: Condens. Matter **18**, 10085 (2006).

[25] M. Lilienblum, T. Lottermoser, S. Manz, S. M. Selbach, A. Cano, and M. Fiebig, Ferroelectricity in the multiferroic hexagonal manganites, Nat. Phys. **11**, 1070 (2015).

[26] B. B. Van Aken, T. T. M. Palstra, A. Filippetti, and N. A. Spaldin, The origin of ferroelectricity in magnetoelectric YMnO$_3$, Nat. Mater. **3**, 164 (2004).

[27] S. Artyukhin, K. T. Delaney, N. A. Spaldin, and M. Mostovoy, Landau theory of topological defects in multiferroic hexagonal manganites, Nat. Mater. **13**, 42 (2014).

[28] Th. Lonkai, D. Hohlwein, J. Ihringer, and W. Prandl, The magnetic structures of $YMnO_{3-\delta}$ and $HoMnO_3$, Appl. Phys. A **74**, s843 (2002).

[29] C. J. Howard, B. J. Campbell, H. T. Stokes, M. A. Carpenter, and R. I. Thomson, Crystal and magnetic structures of hexagonal $YMnO_3$, Acta Crystallogr. B **69**, 534 (2013).

[30] D. G. Tomuta, S. Ramakrishnan, G. J. Nieuwenhuys, and J. A. Mydosh, The magnetic susceptibility, specific heat and dielectric constant of hexagonal $YMnO_3$, $LuMnO_3$ and $ScMnO_3$, J. Phys.: Condens. Matter **13**, 4543 (2001).

[31] M. Giraldo, Q. N. Meier, A. Bortis, D. Nowak, N. A. Spaldin, M. Fiebig, M. C. Weber, and T. Lottermoser, Magnetoelectric coupling of domains, domain walls and vortices in a multiferroic with independent magnetic and electric order, Nat. Commun. **12**, 3093 (2021).

[32] S. Lee, A. Pirogov, M. Kang, K.-H. Jang, M. Yonemura, T. Kamiyama, S.-W. Cheong, F. Gozzo, N. Shin, H. Kimura, Y. Noda, and J.-G. Park, Giant magnetoelastic coupling in multiferroic hexagonal manganites, Nature **451**, 805 (2008).

[33] I. V. Solovyev, M. V. Valentyuk, and V. V. Mazurenko, Magnetic structure of hexagonal $YMnO_3$ and $LuMnO_3$ from a microscopic point of view, Phys. Rev. B **86**, 054407 (2012).

[34] C. Degenhardt, M. Fiebig, D. Fröhlich, Th. Lottermoser, and R. V. Pisarev, Nonlinear optical spectroscopy of electronic transitions in hexagonal manganites, Appl. Phys. B **73**, 139 (2001).

[35] F. Lichtenberg, Presentation of a laboratory for the synthesis and study of special oxides and melt-grown crystalline materials, Report, ETH Zurich (2017).

[36] U. Staub, Y. Bodenthin, C. Piamonteze, S. P. Collins, S. Koohpayeh, D. Fort, and S. W. Lovesey, Magnetoelectric effects studied by resonant x-ray diffraction in ferrimagnetic $GaFeO_3$, Phys. Rev. B **82**, 104411 (2010).

[37] U. Flechsig, F. Nolting, A. Fraile-Rodriguez, J. Krempasky, C. Quitmann, T. Schmidt, S. Spielmann, D. Zimoch, R. Garrett, I. Gentle, K. Nugent, and S. Wilkins, Performance measurements at the SLS SIM beamline, in *SRI 2009, 10th International Conference on Radiation Instrumentation*, edited by R. Garrett, I. Gentle, K. Nugent, and S. Wilkins, AIP Conf. Proc. No. 1234 (AIP, New York, 2010), p. 319.

[38] H. Renevier, J. L. Hodeau, P. Wolfers, S. Andrieu, J. Weigelt, and R. Frahm, Selective Study of Fe Atoms at the Interfaces of an Fe/Ir(100) Superlattice by Means of Diffraction Anomalous Fine Structure, Phys. Rev. Lett. **78**, 2775 (1997).

[39] U. Staub, O. Zaharko, H. Grimmer, M. Horisberger, and F. d'Acapito, Real-part EXAFS from multilayer Bragg reflections: A promising new EXAFS technique, Europhys. Lett. **56**, 241 (2001).

[40] J. P. Hill and D. F. McMorrow, Resonant exchange scattering: Polarization dependence and correlation function, Acta Crystallogr. A **52**, 236 (1996).

[41] Y. Joly, O. Bunău, J. E. Lorenzo, R. M. Galéra, S. Grenier, and B. Thompson, Self-consistency, spin-orbit and other advances in the FDMNES code to simulate XANES and RXD experiments, J. Phys.: Conf. Ser. **190**, 012007 (2009).

[42] T. Lonkai, Elektrische und magnetische Ordnungsparameter im multiferroischen hexagonalen RMnO3-System, PhD. thesis, Eberhard-Karls-Universität Tübingen, 2004.

[43] A. Muñoz, J. A. Alonso, M. J. Martínez-Lope, M. T. Casáis, J. L. Martínez, and M. T. Fernández-Díaz, Magnetic structure of hexagonal $RMnO_3$(R = Y, Sc): Thermal evolution from neutron powder diffraction data, Phys. Rev. B **62**, 9498 (2000).

[44] T. N. Tošić, Q. N. Meier, and N. A. Spaldin, Influence of the triangular MnO breathing mode on magnetic ordering in multiferroic hexagonal manganites, Phys. Rev. Res. **4**, 033204 (2022).

[45] K. H. Wu, H.-J. Chen, C. C. Hsieh, C. W. Luo, T. M. Uen, J.-Y. Lin, and J. Y. Juang, Epitaxial-strain effects on electronic structure and magnetic properties of hexagonal $YMnO_3$ thin films studied by femtosecond spectroscopy, J. Supercond. Novel Magn. **26**, 801 (2013).

[46] S. Di Matteo, Y. Joly, and C. Natoli, Detection of electromagnetic multipoles by x-ray spectroscopies, Phys. Rev. B **72**, 144406 (2005).

[47] R. Sessoli, M.-E. Boulon, A. Caneschi, M. Mannini, L. Poggini, F. Wilhelm, and A. Rogalev, Strong magneto-chiral dichroism in a paramagnetic molecular helix observed by hard x-rays, Nat. Phys. **11**, 69 (2015).

[48] M. Ramakrishnan, Investigation of Magnetoelectric Properties with X-rays, PhD thesis, ETH Zurich (2017).

[49] S. W. Lovesey, E. Balcar, K. S. Knight, and J. Fernandez Rodriguez, Electronic properties of crystalline materials observed in x-ray diffraction, Phys. Rep. **411**, 233 (2005).

[50] L. P. Kadanoff, W. Götze, D. Hamblen, R. Hecht, E. A. S. Lewis, V. V. Palciauskas, M. Rayl, J. Swift, D. Aspnes, and J. Kane, Static phenomena near critical points: Theory and experiment, Rev. Mod. Phys. **39**, 395 (1967).

[51] A. Say, O. Mys, D. Adamenko, A. Grabar, Y. Vysochanskii, A. Kityk, and R. Vlokh, Critical exponents of phase transition in ferroelectric $Sn_2P_2S_6$: Comparison of optical and dilatometric data, Phase Trans. **83**, 123 (2010).

[52] C. K. Sarikaya and H. Yurtseven, Temperature dependence of the spontaneous polarization near the ferroelectric-paraelectric transition in $NaNO_2$, High Temp. Mater. Process. **32**, 77 (2013).

[53] U. Staub, L. Rettig, E. M. Bothschafter, Y. W. Windsor, M. Ramakrishnan, S. R. V. Avula, J. Dreiser, C. Piamonteze, V. Scagnoli, S. Mukherjee, C. Niedermayer, M. Medarde, and E. Pomjakushina, Interplay of Fe and Tm moments through the spin-reorientation transition in $TmFeO_3$, Phys. Rev. B **96**, 174408 (2017).

Correction: The sixth sentence of the first paragraph of Sec. IV D contained an incorrect term and has been fixed.